ORIGINAL

Konstantin Naumenko · Behnaz Bagheri

A direct approach to evaluate interaction forces between self-adhesive polymeric films subjected to T-peeling

Abstract In this paper, a direct procedure to identify interaction forces between self-adhesive flexible polymeric films is developed. High-resolution photographs of the deformed shape within and outside the zone of adhesive interaction are taken at different instances of the T-peel test. To describe the deformed centerline, an approximate analytical solution to the equations of the nonlinear beam theory is derived. The obtained function is the exponential sum satisfying both kinematic and static boundary conditions for the T-peel configuration. The interaction forces computed with the developed function satisfy equilibrium conditions. The procedure provides characteristics of the adhesive interaction such as the energy of adhesion, maximum force and critical opening displacement. Furthermore, the developed direct approach is applicable to generate the whole traction–separation curve.

1 Introduction

Adhesive flexible films are widely used in many industry branches, for example multifunctional layered devices [5,6,34], photovoltaic and glass laminates [8,9,24,32] as well as packaging, protection and transportation [19,20]. In application to the packaging, the important properties of films include strength of the sealed seam and peel ability. On the one hand, the films and the sealing seam must meet the given strength requirements such that the integrity of the packaging is guaranteed. On the other hand, the packaging must be easily peelable, i.e., it must be possible to open it by hand applying a small force. For the optimal design of a packaging system, for the selection of materials and the evaluation of functionality, a thorough understanding of a peeling process, a problem-oriented modeling and analysis of the composite strength, and robust computational methods are required.

The opening of peeling systems is a complex fracture mechanical process for which a closed relationship between manufacturing conditions, microstructure and strength properties does not yet exist [21]. In practice, experiments are performed to determine the peel force of a given system. Examples include T-peel tests [22], V-peel tests [18] and fixed-arm peel tests [23]. However, most standardized test methods do not give direct access to the adhesion properties, such as adhesion energy, critical opening displacement and maximum adhesion force. They also provide only limited insights into the adhesion mechanisms of the composite. For this reason, advanced measuring methods have been developed in recent years to investigate the behavior of the process

K. Naumenko (✉) · B. Bagheri
Otto-von-Guericke-University Magdeburg, Institute of Mechanics, Universitätsplatz 2, 39106 Magdeburg, Germany
E-mail: konstantin.naumenko@ovgu.de

B. Bagheri
E-mail: behnaz.bagheri@ovgu.de

zone during the peeling process. Examples are digital image correlation (DIC) systems [11,30] and in situ X-ray tomography [27].

The widely used approach in analysis of peel systems is to formulate a constitutive equation for the interaction force as a function of the opening displacement. Traction–separation laws (also known as cohesive or adhesive zone models) were developed in the fracture mechanics [25,26]. The crucial point is the identification of parameters in the traction–separation law from the results of peel tests. The standard procedure is to assume a specific idealized shape of the traction–separation curve, like rectangular, triangular, polynomial or exponential [25,26], to simulate a peel test and to identify parameters by the comparison of the computed force–displacement diagram with the experimental one, e.g., [19]. Once the traction–separation law is given, the peeling process can be simulated applying a finite element code by meshing the interaction zone with cohesive elements; see, e.g., [13,16,19,31].

In many applications, the type of the traction–separation law is not known a priori. An example is the peeling of self-adhesive thin polymeric films having relatively long-range force interactions [3,22]. In this case, it is useful to generate the traction–separation curve from the results of measurements. Based on the curve a suitable, possibly non-local constitutive law should be formulated and identified. To obtain a traction–separation curve, digital images of the deformed film and/or results of DIC measurements of deformation fields inside and outside the adhesive process zone must be available from peel tests. Then the forces required to produce the given deformation can be evaluated applying the theories of beams, plates and shells.

In order to compute the interaction force distribution, experimental data on the deformed configuration must be approximated such that higher-order derivatives are accessible. A classical example is a small deflection of a double cantilever beam, where the fourth-order derivative of the deflection function is required to compute the distributed force. As discussed in [22], the standard approaches, for example polynomial series, B-splines, etc., can be used to approximate the deformed line of the film $y(x)$ and its first derivative $y'(x)$ with satisfactory accuracy. However, significant errors are obtained by computing the higher-order derivatives. In [22], the local curvature of a thin film is evaluated numerically applying the power series approximation for the deflection of the centerline. The results show non-physical oscillations and are not applicable to compute the adhesive forces. For this reason, the direct approach to evaluate the traction–separation cure was usually rejected in the previous studies [3,22].

In this paper, we address an alternative procedure to describe the deformed centerline of the film. To this end, an approximate analytical solution to the equations of the nonlinear beam theory will be derived and utilized to fit the deformation curves from experiments. High-resolution photographs of the deformed shape within and outside the zone of adhesive interaction at different instances of T-peel test will be applied. An important feature of the developed approximations is that they satisfy kinematic and static boundary conditions for the T-peeling. Furthermore, the obtained interaction forces satisfy equilibrium conditions. The results of the proposed direct approach will we compared with those based on the direct variational methods discussed in the literature.

2 Governing equations

Figure 1a illustrates flexible films subjected to T-peel loading. Under the assumption of slow quasi-static peeling, the horizontal forces in the clamps are negligible. Furthermore, as long as the peel configuration remains symmetric, i.e., the deformed configuration of the lower film is the mirror reflection of the upper one, the horizontal components of the interaction forces do not arise.

Figure 1b illustrates qualitatively the distributed interaction force q between the films. One feature is the long-range force interaction usually both inside and outside the contact zone. For cohesive peel systems, for example low-density polyethylene/isotactic polybutene-1 films, micro-crazes and fibrils are usually formed in the process zone [21]. In this paper, adhesive peel systems are considered. In this case, no process zone could be recognized, even with electron microscopy. Nevertheless, relatively long-range interactions are identified in [22]. Entanglement of single polymer chains, adsorption and electrostatic forces can be assumed as mechanisms of interaction. The aim of this paper is to identify the distributed force q due to these mechanisms from the deformed line of the peel arm. In this section, we present governing equations to describe the equilibrium configurations of thin flexible films. To this end, the nonlinear theory of inextensible rods [1,2] will be applied.

Let s be the arc-length parameter in the deformed state characterizing positions of cross sections of the deformed film and let x and y be the corresponding Cartesian coordinates (Fig. 1).

The actual orientation of any cross section is described by the angle $\psi(s)$ (Fig. 2), while $\varphi(s)$ is the angle between the tangent to the deformed line and the x-axis.
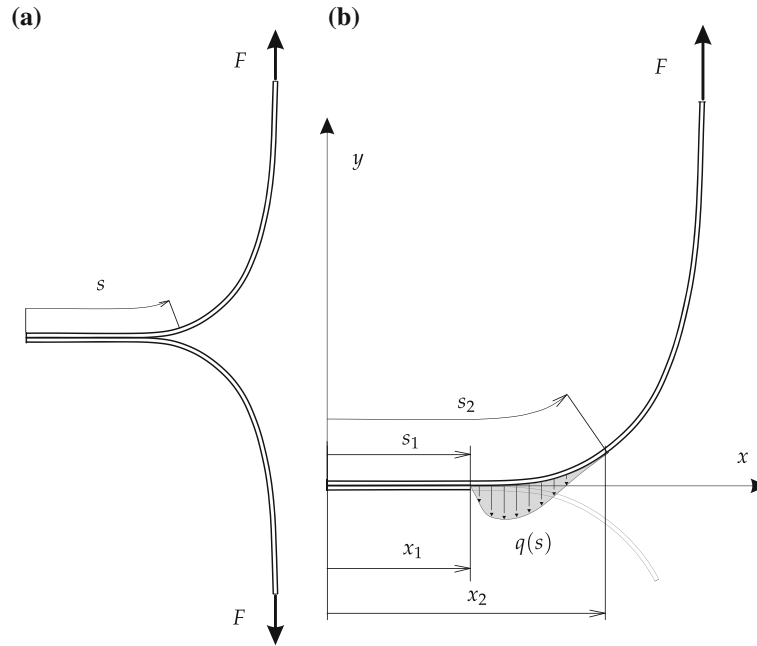
Fig. 1 Deformed configuration of films subjected to T-peeling. **a** Loading and deformed shape, **b** force distribution within the zone of adhesive interaction
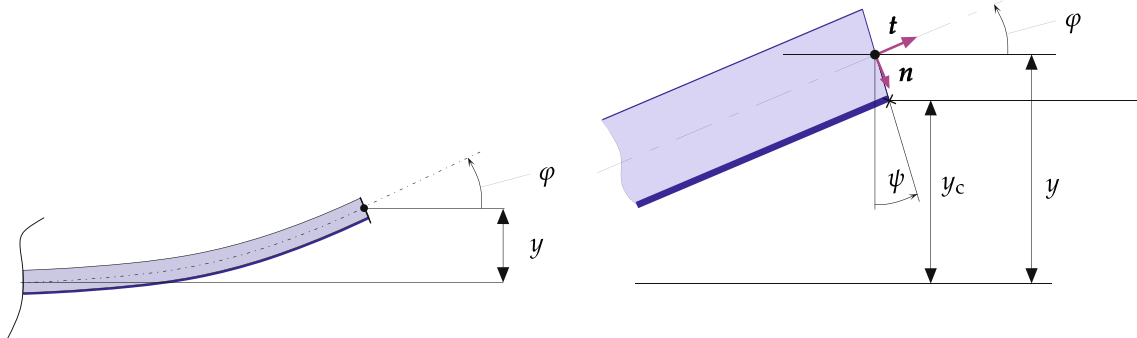
Fig. 2 Cross section with the coordinate s

The tangent and the normal unit vectors to the deformed centerline are specified by $\boldsymbol{t}$ and $\boldsymbol{n}$, respectively. For a cross section with coordinates x, y and the rotation angle ψ, the lower point of the cling layer is defined by the following coordinates (Fig. 2)

$$x_c = x - \frac{h}{2}\sin\psi, \quad y_c = y - \frac{h}{2}\cos\psi \tag{1}$$

The following kinematical relations are valid

$$\frac{dy}{ds} = \sin\varphi, \quad \frac{dx}{ds} = \cos\varphi, \quad y' = \tan\varphi, \quad (\ldots)' = \frac{d(\ldots)}{dx} \tag{2}$$

Figure 3 illustrates a free body diagram for a part of a film defined by the coordinates s_1 and s_2 within the adhesive zone.

The mechanical interactions between the cross sections are characterized by the normal force N, the shear force Q and the bending moment M. Applying the balances of forces and moments for the line element with arbitrary coordinates s_1 and s_2, the following equilibrium conditions can be derived

$$\frac{dH}{ds} = 0, \quad \frac{dV}{ds} = -q, \quad \frac{dM}{ds} = Q + \frac{h}{2}q\sin\psi, \tag{3}$$
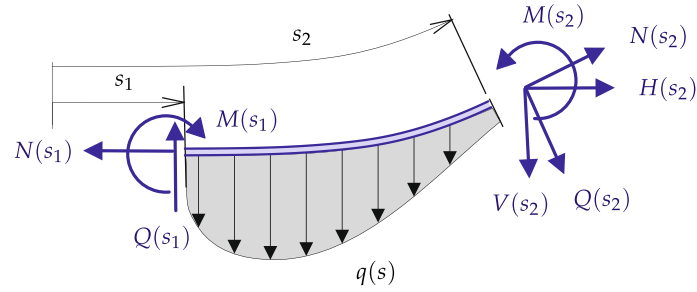
Fig. 3 Free body diagram for a part of the film inside the zone of adhesive interaction

where H is the horizontal and V the vertical component of the force vector, respectively. Integrating Eq. (3)$_1$ provides $H = $ const, and the integration constant is zero since the force F is applied in the vertical direction. With $H = 0$, both the following relations for the normal and the shear force can be established

$$N = -V \sin \varphi, \quad Q = V \cos \varphi \tag{4}$$

For the analysis of T-peeling, let us apply the theory of inextensible rods [2] by assuming that the axial strain of the centerline is negligible. Below this assumption will be justified based on photographs of the deformed shape of the peel arm. For the shear force and the bending moment, the constitutive equations can be formulated as follows

$$M = \frac{\partial W}{\partial (\chi)}, \quad \chi = \frac{\mathrm{d}\psi}{\mathrm{d}s},$$
$$Q = \frac{\partial W}{\partial \gamma}, \quad \gamma = \psi - \varphi, \tag{5}$$

where W is the strain energy density per unit length of the undeformed film, χ is the curvature and γ is the transverse shear strain. By specifying the strain energy density, Eqs. (2)–(5) together with boundary conditions can be applied to find the deformed configuration of the beam for the known forces F and q. Vice versa, if y, λ and ψ are known then the distributed adhesive force q can be evaluated from Eqs. (2)–(5).

For the distributed force q, we assume that a potential $\mathcal{U}$ exists such that

$$q = \frac{\mathrm{d}\mathcal{U}}{\mathrm{d}y_c} \tag{6}$$

The strain energy density is a function of three arguments including χ, γ and ψ. Taking its derivative with respect to the coordinate s and applying constitutive equations (5), we obtain

$$\frac{\mathrm{d}W}{\mathrm{d}s} = N \frac{\mathrm{d}}{\mathrm{d}s} + Q \frac{\mathrm{d}\gamma}{\mathrm{d}s} + M \frac{\mathrm{d}\chi}{\mathrm{d}s} \tag{7}$$

With Eqs. (3)–(5), (7) takes the following form

$$\frac{\mathrm{d}}{\mathrm{d}s}(W - M\chi - N) = -q \frac{\mathrm{d}y_c}{\mathrm{d}s} \tag{8}$$

Equation (8) is the conservation law for the nonlinear beam theory. Within the three-dimensional theory of elasticity, similar Eshelby-type conservation laws are discussed in [15,17].

Taking into account Eq. (6), the following integral of Eq. (8) can be derived

$$W + \mathcal{U} - M\chi - N = C, \tag{9}$$

where C is a constant. In [22], it is shown that by analogy to the J-integral in fracture mechanics the quantity $\Gamma = M\chi + N - W$ provides the energy release rate for T-peeling of flexible films. For $s = l$, we obtain $\Gamma(l) = F$. Therefore, the following relationship between the peel force F_{peel} and the specific energy of adhesion Υ is derived

$$F_{\text{peel}} = \Upsilon b, \tag{10}$$

where b is the width of the film. Equation (10) was derived by Rivlin [29] for inextensible films. Let us note that the integral of the type (9) can also be derived for hyperelastic films undergoing finite axial deformations. The generalized relationship for the work of adhesion is presented in [10].
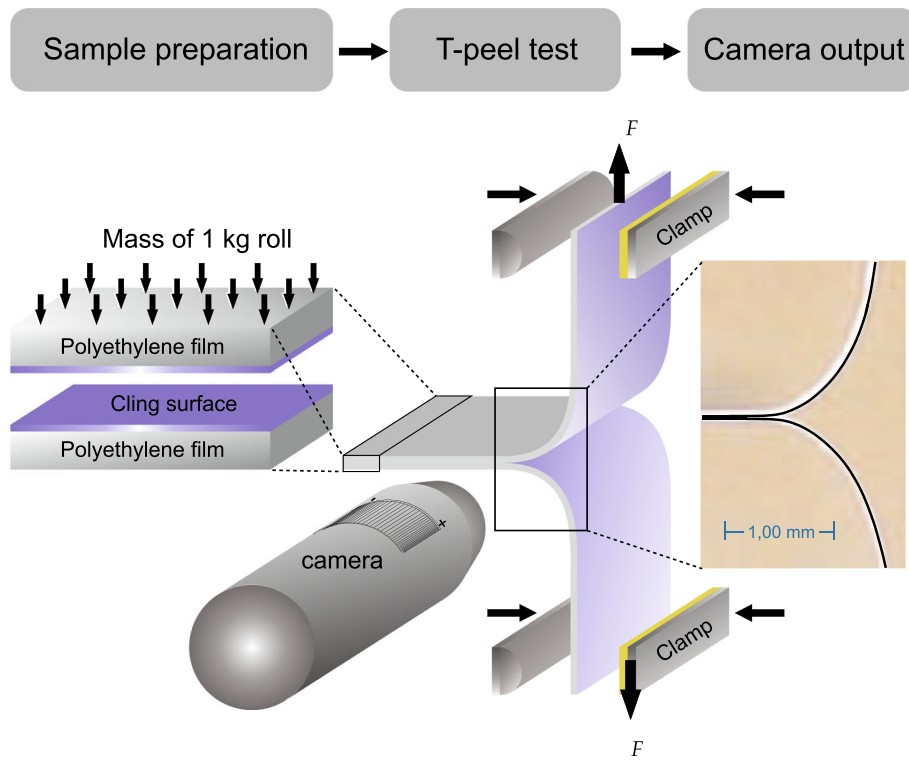
**Fig. 4** Schematic of T-peel test configuration

3 Experimental setup

Figure 4 illustrates the sketch of the T-peel configuration and the constituent layers of the films. The films with the thicknesses of 23 μm were fabricated from polyethylene. They exhibit self-adhesive behavior because of the coextruded polymer cling material. The T-peel tests were performed according to the ASTM 1876 standard applying a Zwick tensile testing machine. The initial distance between the clamps was 60mm with the peel rate of 100 mm/min. For sample preparation, two similar polymer films were pressed to each other by a roll with the mass of 1 kg. The dimensions of the specimens were $b = 25$mm and $l = 65$mm. Videos of the peeling were recorded with a digital USB microscope camera (frame rate of 10 frames/s). The camera was located perpendicular to the transverse view of the specimen and the grips during the peel test (Fig. 4). The results of peel tests are presented as the measured force vs opening diagrams, providing the value of the peel force F_{peel} as illustrated in Fig. 5. In addition, photographs of the deformed configuration were taken at different time instances during the peeling. From the self-adhesive polyethylene film with the thickness of 23 μm , 5 samples were prepared to be tested under T-peeling. The whole test procedure of each test was recorded by a microscopic camera which provided the deformation pictures of the films. Finally, from each test 5 pictures were randomly chosen to be evaluated. Figure 6 illustrates the approximation of the average deformation centerline, and the light blue range represents the variations in the film deformation in 25 pictures from 5 tests. From the images, the deformed centerlines of the film were approximated by the B-spline technique applying Rhino® software. Figure 6 shows the approximations results and the averaged centerline which will be used for the identification.

4 Procedure to identify interaction forces

In order to formulate the robust identification procedure, let us simplify (2)–(5) applying the following assumption. The deformed centerlines obtained from tests show that the thickness of the film is much less than the length of the film within the zone of non-zero curvature. Furthermore, for the considered T-peeling we expect that the transverse shear deformation is small and can be neglected. Therefore, in this study we apply the shear rigid model, by setting $\gamma = 0$.
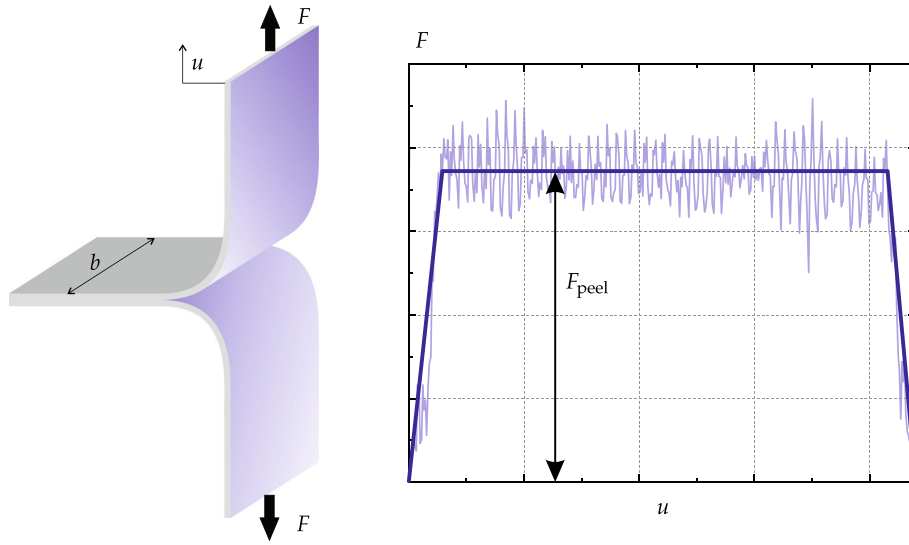
Fig. 5 Idealized force vs opening diagram for pell force evaluation
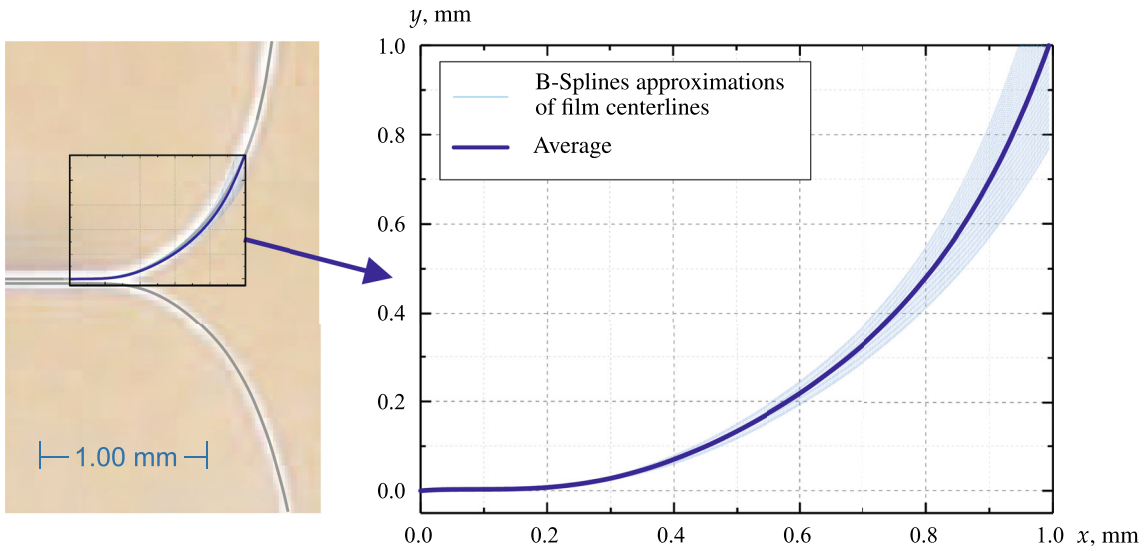
Fig. 6 Approximations of deformed centerlines

Setting $\psi = \varphi$ and applying Eq. (2), the local curvature can be expressed as follows

$$\chi = \frac{\mathrm{d}\varphi}{\mathrm{d}s} = \frac{\mathrm{d}(\sin\varphi)}{\mathrm{d}x} = -\frac{\mathrm{d}(\cos\varphi)}{\mathrm{d}y} \tag{11}$$

Assuming the linear elastic response of the peel arm, the bending moment is proportional to the curvature

$$M = B\chi, \tag{12}$$

where B is the bending stiffness. With the assumed small strain ε and negligible transverse shear deformation, Eq. (9) yields

$$\mathcal{U} - \frac{1}{2}M\chi - N = C \tag{13}$$

Applying the boundary conditions $N = 0$, $M = 0$ and setting $\mathcal{U} = 0$ for the left free edge of the film, we obtain $C = 0$ and

$$\mathcal{U} = \frac{1}{2}M\chi + N \tag{14}$$

Specifying $\Omega = \cos\varphi$, the following expressions can be derived from Eqs. (2)–(6) and (12)

$$M = -B\Omega^{\bullet}, \quad N = B\frac{1-\Omega^2}{\Omega}\Omega^{\bullet\bullet},$$

$$V = -B\frac{\sqrt{1-\Omega^2}}{\Omega}\Omega^{\bullet\bullet},$$

$$\mathcal{U} = B\left[\frac{1}{2}\Omega^{\bullet 2} + \frac{1-\Omega^2}{\Omega}\Omega^{\bullet\bullet}\right], \tag{15}$$

where

$$(\ldots)^{\bullet} = \frac{\mathrm{d}(\ldots)}{\mathrm{d}y}$$

In order to compute the interaction force distribution $q(y)$, we need to approximate the function $\Omega(y)$ from the deformed configuration of the beam centerline. High-quality vector images of the deformed films and B-spline approximations provide both the deformed line $y(x)$ and its first derivative $y'(x)$ with satisfactory accuracy. However, the experimental curves generated from images usually have a scatter of the order of magnitude of the film thickness. This leads to the loss of accuracy by computing the higher derivatives. As shown in [22], non-physical oscillations are observed for the curvature, if the deformed centerline is approximated by polynomials. Due to the fact that third derivatives are required to compute the force potential $\mathcal{U}$, the direct approach was rejected in [3,22].

An alternative procedure could be to approximate the deformed line based on the equations of the beam theory. However, closed-form solutions to Eqs. (2)–(6) are only available for the geometrically linear case (small strains and cross-sectional rotations) and special types of the traction–separation laws, e.g., linear, triangular or piecewise linear laws [7,33].

To derive a suitable approximation for the function $\Omega(y)$, let us assume that for a part of the beam the interaction force is negligible. By setting $q = 0$, Eq.(3)$_2$ can be integrated providing $V = $ const. With the boundary conditions for $s = l$, we obtain the vertical force $V = -F_{\mathrm{peel}}$. The normal force is computed from Eq. (4)$_1$ as follows

$$N = F_{\mathrm{peel}}\sin\varphi \tag{16}$$

For $q = 0$, the force potential takes the constant value $\mathcal{U} = \mathcal{U}_0$. The energy integral (14) takes the form

$$\mathcal{U}_0 = \frac{1}{2}M\chi + F_{\mathrm{peel}}\sin\varphi \tag{17}$$

With the boundary condition $M = 0$ for $s = l$ and $\varphi = \pi/2$, we obtain $\mathcal{U}_0 = F_{\mathrm{peel}}$. Taking into account Eq. (12), the energy integral (17) can be formulated as follows

$$\frac{1}{2}B\chi^2 = F_{\mathrm{peel}}(1 - \sin\varphi) \tag{18}$$

Let us note that Eq. (18) is known as the energy integral of Euler's elastica; see, for example, [2]. It can be used to compute the function Ω for the part of the film. Indeed from Eq. (18), we obtain

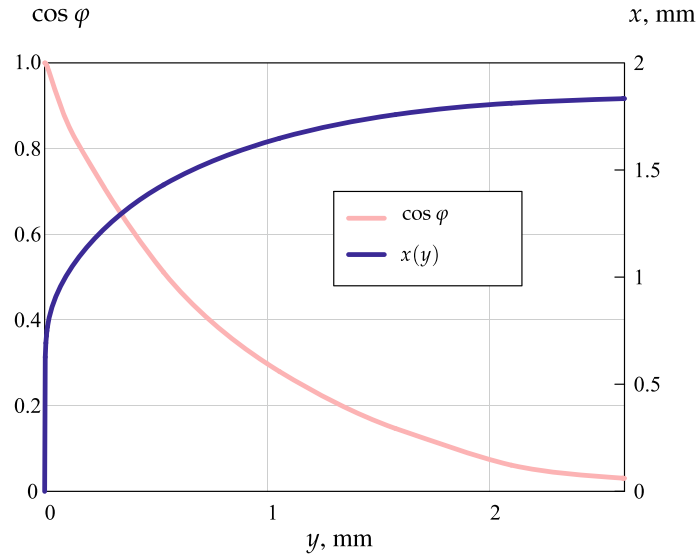$$\frac{1}{2}B\Omega^{\bullet 2} = F_{\mathrm{peel}}(1 - \sqrt{1-\Omega^2}) \tag{19}$$

Taking into account that Ω is a decreasing function, we obtain

$$\Omega^{\bullet} = -\sqrt{2\tilde{F}_{\mathrm{peel}}}\left(1 - \sqrt{1-\Omega^2}\right)^{1/2}, \quad \tilde{F}_{\mathrm{peel}} = \frac{F_{\mathrm{peel}}}{B} \tag{20}$$

By integration, the following relation between Ω and y is derived

$$\Psi(\Omega) = \sqrt{2\tilde{F}_{\mathrm{peel}}}(y - y_0), \quad \Psi(\Omega) = \int_{\Omega_0}^{\Omega}\frac{d\xi}{\left(1 - \sqrt{1-\xi^2}\right)^{1/2}}, \quad \Omega_0 = \cos\varphi_0 \tag{21}$$

Fig. 7 Functions $x(y)$ and $\cos\varphi(y)$ identified from digital images of centerline

where y_0 and φ_0 are the opening and the corresponding angle of rotation for a point of the beam with the coordinate s_0. The integral in $\Psi(\Omega)$ can be formulated in a closed analytical form in terms of elliptic functions. For the purpose of the identification, it is useful to approximate the solution (21) by the use of elementary functions. Indeed the solution (21) is only valid for a part of the beam where the interaction forces are negligible. For this part, the angle of rotation is close to $\pi/2$ and we can assume $\Omega^2 \ll \Omega < 1$. In this case, the differential equation (21) takes the simplified form

$$\Omega^\bullet = -\sqrt{\tilde{F}_{\text{peel}}}\,\Omega, \tag{22}$$

with the solution

$$\Omega(y) = A\exp(-\alpha y), \quad \alpha = \sqrt{\tilde{F}_{\text{peel}}} \tag{23}$$

where A is the integration constant. The function (23) approximates the cross-sectional rotation only for a part of the beam and satisfies the boundary condition $N = F_{\text{peel}}$ for the top right edge. To improve the accuracy, let us assume the following two-term approximation

$$\Omega(y) = A\exp(-\alpha y) + B\exp(-\beta y), \quad \beta > \alpha \tag{24}$$

Applying the boundary conditions for the left edge of the beam $\Omega(0) = 1$ and $\Omega^\bullet(0) = 0$, we obtain

$$A = \frac{\beta}{\beta - \alpha}, \quad B = -\frac{\alpha}{\beta - \alpha}$$

To find β, the least-squares method can be applied.

Figure 7 illustrates the plots of functions $x(y)$ and $\cos\varphi(y)$.

For the identification, the centerline of the film was digitized from a photograph applying Rhino® software. With the B-spline approximations of $y(x)$ the first derivative $y'(x)$ and the function

$$\cos\varphi = \frac{1}{\sqrt{1 + y'^2}}$$

were evaluated numerically. Figure 8 illustrates the approximations according to the closed-form solution (21) for the beam without the interaction forces. With the normalized peel force $\tilde{F}_{\text{peel}} = 3.23$ and by setting $y_0 = 2.6$ mm, $\Omega_0 = 0.03$ the closed-form solution agrees well with experimental data for the right part of the beam having the opening within the range 1.6 mm $< y <$ 2.6 mm. For the same peel force but with $y_0 = 0.02$ mm and $\Omega_0 = 0.98$, the solution meets well the experimental data for the right edge of the beam as well as for the openings within the range 0.02 mm $< y <$ 0.04 mm (Fig. 9). Plots of the exponential approximation (23) with the same peel force and $A = 1.013$ are presented in Figs 8 and 9. We observe that the exponential
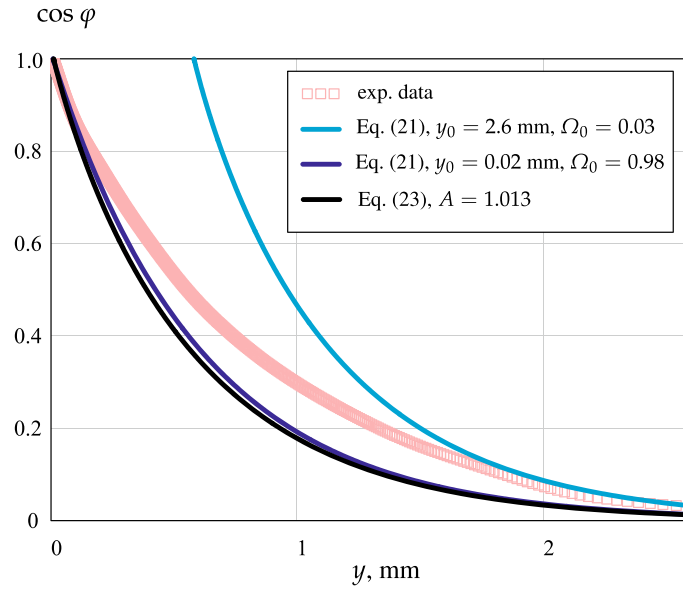
Fig. 8 Function $\cos\varphi(y)$ identified from digital images of centerline and approximated by Eqs. (21) and (23)
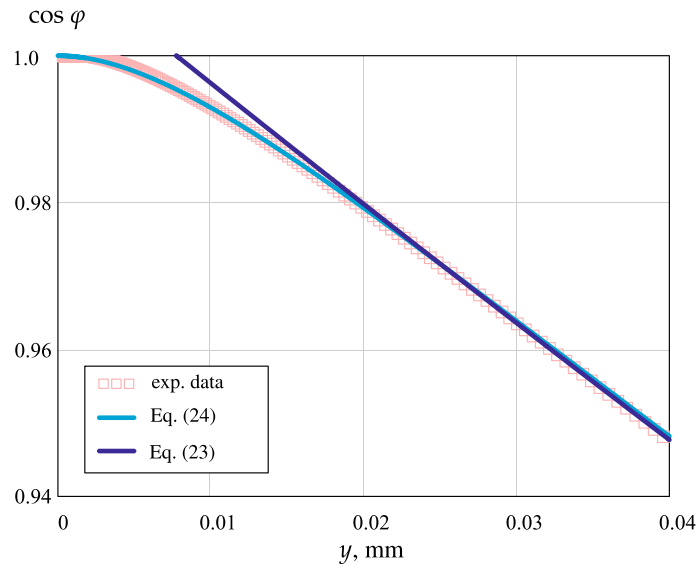

Fig. 9 Function $\cos\varphi(y)$ identified from digital images of centerline and approximated by Eqs (23) and (24)

approximation almost coincides with the closed-form solution for $y_0 = 0.02$ mm and $\Omega_0 = 0.98$ (Fig. 8). Let us note that both the closed-form solution and the single-term approximation describe the function $\cos\varphi$ for a clamped cantilever beam without adhesive interaction. These approximations do not agree with experimental data for the left part of the beam (Fig. 9). Applying the two-term exponential sum (24), the boundary conditions for the left edge of the beam are satisfied. With $\beta = 127$, the function $\cos\varphi$ for a wide range of openings y is well approximated (Fig. 9).

With the proposed functions $\Omega(y)$, the distributed interaction force q can be now computed as follows

$$q = B\left[-\frac{1}{\Omega^2}\Omega^{\bullet\bullet}\Omega^{\bullet} + \frac{1 - \Omega^2}{\Omega}\Omega^{\bullet\bullet\bullet} \right] \tag{25}$$

Figure 10 illustrates the results of identification applying the single-term and two-term exponential approximations. As expected, the single-term approximation (23) leads to the negligible interaction forces for the whole beam. The two-term exponential sum (23) provides the physically correct distribution of q vs y.
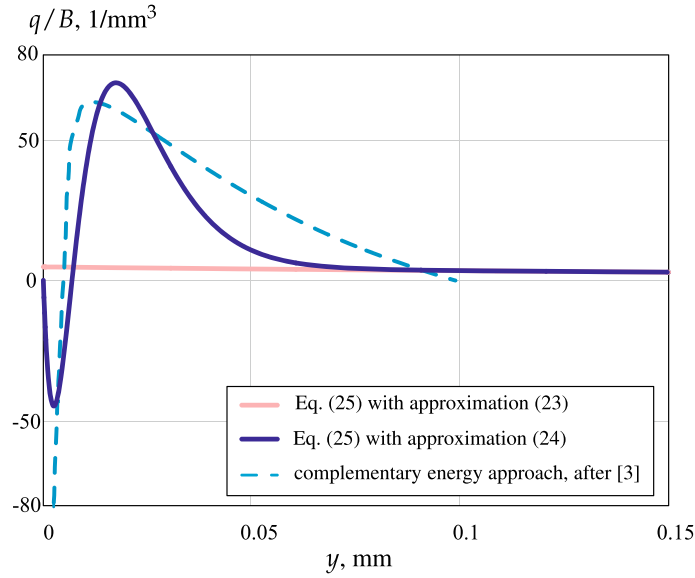
Fig. 10 Interaction distributed forces q vs opening y evaluated different approaches

Both the maximum force $q_{\max}/B = 72$ 1/mm^3 and the critical opening $y_* \approx 0.075$ mm are identified. The obtained values indicate that self-adhesive polymeric films exhibit a relatively long-range interaction forces. Long-range force interactions were also identified in [3,22] for similar cling materials. In [3], the distributed force q was approximated by the power series with respect to the x-coordinate and the coefficients in the series were computed from the complementary energy variational functional by the Ritz method. For the comparison, the results obtained in [3] are plotted in Fig. 10 by the dashed line. We observe that the maximum force and the critical opening agree approximately by the direct and the complementary energy approaches.

Equation (25) provides q as a function of the separation y. In order to compute the force distribution along the arc-length parameter s, the function $s(y)$ is required. From Eq. (2)$_1$, the following differential equation can be derived

$$s^\bullet = \frac{1}{\sin\varphi} = \frac{1}{\sqrt{1-\Omega^2}} \tag{26}$$

After integration, we obtain

$$s(y) = \int\limits_0^y \frac{\mathrm{d}\xi}{\sqrt{1-\Omega^2(\xi)}}$$

The interaction forces identified with the exponential sum (23) satisfy the equilibrium conditions. Indeed the equilibrium condition for the forces can be formulated as follows

$$\int\limits_0^l q(s)\mathrm{d}s = F_{\mathrm{peel}} \tag{27}$$

With Eqs. (3) and (15), we obtain

$$\int\limits_0^l q(s)\mathrm{d}s = -\int\limits_0^l \frac{\mathrm{d}V}{\mathrm{d}s}\mathrm{d}s = V(0) - V(l) = B\frac{\sqrt{1-\Omega^2}}{\Omega}\Omega^{\bullet\bullet}\Big|_{y=0}^{y=y_{\max}}$$

For $y = 0$, we have $\Omega = 1$, while for $\beta y \gg 1$

$$\Omega(y) = \frac{\beta}{\beta-\alpha}\exp(-\alpha y), \quad \Rightarrow \quad \frac{\Omega^{\bullet\bullet}}{\Omega} = \alpha^2 = \tilde{F}_{\mathrm{peel}}$$

Consequently, for $y = y_{\max}$

$$\frac{\sqrt{1 - \Omega^2}}{\Omega} \Omega^{\bullet\bullet} = \tilde{F}_{\text{peel}},$$

and Eq. (27) is satisfied. On the other hand, taking the top right point of the beam as the reference point, the equilibrium condition for the moments takes the form

$$\int_0^l q(s)(x_l - x) \mathrm{d}s = F_{\text{peel}} \frac{h}{2}, \tag{28}$$

where x_l is the x-coordinate of the right top point of the beam. With Eqs (3) and (15) and by integration by parts, we obtain

$$\int_0^l q(s)(x_l - x)\mathrm{d}s = V(0)x_l - \int_0^{x_l} V \mathrm{d}x = V(0)x_l - M(x_l) + M(0) + \frac{h}{2} \int_0^{y_{\max}} q \mathrm{d}y$$

With $\mathrm{d}y_c = (1 + \chi h/2)\mathrm{d}y \approx \mathrm{d}y$ and

$$\int_0^{y_{\max}} q\mathrm{d}y = \int_0^{y_{\max}} \frac{\mathrm{d}\mathcal{U}}{\mathrm{d}y_c}\mathrm{d}y \approx \mathcal{U}(y_{\max}) - \mathcal{U}(0) = F_{\text{peel}}$$

we finally obtain

$$\int_0^l q(s)(x_l - x)\mathrm{d}s - F_{\text{peel}}\frac{h}{2} = V(0)x_l - M(x_l) + M(0) \tag{29}$$

For the two-term exponential sum (24), the boundary conditions $V(0) = 0$, $M(0) = 0$ and $M(y_{\max}) = 0$ are satisfied. Therefore, the derived interaction force q satisfies the equilibrium condition (28).

Equations (23) and (24) are special cases of the exponential sum which can be applied to approximate a function $f(x)$ as follows

$$f(x) = \sum_{k=1}^n A_k \exp(\mu_k x) \tag{30}$$

Applications of exponential sums in various physics and engineering problems as well as algorithms to compute coefficients A_k and exponents μ_k are discussed in [4,14,28], among others. For the problem considered in this paper, the two-term sum (24) is applied and the adding of an additional exponential term does not lead to an improvement of approximation. Indeed, to identify constants in higher-order exponential terms photographs within the process zone of peeling with higher resolution are required. Furthermore, the applied shear rigid beam theory may lead to inaccurate results as the length of the analyzed process zone becomes comparable with the film thickness.

5 Conclusions

An important step in the analysis of adhesive strength and delamination in layered systems is to identify traction–separation behavior. To this end, a traction–separation law should be formulated and identified from experimental data.

This paper addresses the direct procedure to evaluate the interaction forces between thin flexible polymeric films within the adhesive zone. Toward this goal, high-resolution photographs of the deformed shape within and outside the zone of adhesive interaction were taken at different time instances during T-peeling. From the digitized images, the deformed centerline is approximated by B-splines and the cross-sectional rotation φ is evaluated numerically. The exponential sum is applied to approximate $\Omega = \cos\varphi$ as the function of the opening y. It satisfies kinematic and static boundary conditions for the T-peel test configuration. Applying the nonlinear theory of shear rigid beams, the force of interaction is evaluated directly by taking the derivatives of the given function Ω. The resulting distribution $q(y)$ satisfies equilibrium conditions for the forces and

moments. Furthermore, it provides the important characteristics of the adhesive interaction including the maximum force and the critical opening.

Based on the results, we may conclude as follows:

– In order to extract the traction–separation curve from the results of T-peel tests, accurate approximation of the deformed peel arm centerline is required. The smooth differentiable approximation function should satisfy kinematic and static boundary conditions as well as equilibrium conditions for both the forces and moments.
– The identified traction–separation curve shows distributed forces outside the contact zone. This indicates the non-locality of the adhesive force interaction between the considered films.

Further studies should be related to formulate an appropriate non-local traction–separation law to describe the adhesive force interactions. Examples are recently discussed within the peridynamics modeling of layered systems [12]. With the developed traction–separation law, simulations of the peel processes should be performed by a finite element code.

References

1. Altenbach, H., Naumenko, K., Zhilin, P.A.: A direct approach to the formulation of constitutive equations for rods and shells. In: Pietraszkiewicz, W., Szymczak, C. (eds.) Shell Structures: Theory and Applications, pp. 87–90. Taylor & Francis, Leiden (2005)
2. Antman, S.: Nonlinear Problems of Elasticity. Applied Mathematical Sciences. Springer, New York (2006)
3. Bagheri, B., Schulze, S.H., Naumenko, K., Altenbach, H.: Identification of traction-separation curves for self-adhesive polymeric films based on non-linear theory of beams and digital images of T-peeling. Compos. Struct. **216**, 222–227 (2019)
4. Beylkin, G., Monzón, L.: Approximation by exponential sums revisited. Appl. Comput. Harmonic Anal. **28**(2), 131–149 (2010)
5. Chiang, C.J., Winscom, C., Bull, S., Monkman, A.: Mechanical modeling of flexible OLED devices. Org. Electron. **10**(7), 1268–1274 (2009)
6. Choi, J.H., Kim, D., Yoo, P., Lee, H.: Simple detachment patterning of organic layers and its application to organic light-emitting diodes. Adv. Mater. **17**(2), 166–171 (2005)
7. Dimitri, R., Cornetti, P., Mantič, V., Trullo, M., De Lorenzis, L.: Mode-I debonding of a double cantilever beam: a comparison between cohesive crack modeling and finite fracture mechanics. Int. J. Solids Struct. **124**, 57–72 (2017)
8. Dupont, S.R., Oliver, M., Krebs, F.C., Dauskardt, R.H.: Interlayer adhesion in roll-to-roll processed flexible inverted polymer solar cells. Sol. Energy Mater. Sol. Cells **97**, 171–175 (2012)
9. Eisenträger, J., Naumenko, K., Altenbach, H., Köppe, H.: Application of the first-order shear deformation theory to the analysis of laminated glasses and photovoltaic panels. Int. J. Mech. Sci. **96**, 163–171 (2015)
10. Eremeyev, V.A., Naumenko, K.: A relationship between effective work of adhesion and peel force for thin hyperelastic films undergoing large deformation. Mech. Res. Commun. **69**, 24–26 (2015)
11. Fedele, R., Raka, B., Hild, F., Roux, S.: Identification of adhesive properties in glare assemblies using digital image correlation. J. Mech. Phys. Solids **57**(7), 1003–1016 (2009)
12. Gao, Y., Oterkus, S.: Fully coupled thermomechanical analysis of laminated composites by using ordinary state based peridynamic theory. Compos. Struct. **207**, 397–424 (2019)
13. Gialamas, P., Völker, B., Collino, R.R., Begley, M.R., McMeeking, R.M.: Peeling of an elastic membrane tape adhered to a substrate by a uniform cohesive traction. Int. J. Solids Struct. **51**(18), 3003–3011 (2014)
14. Holmström, K., Petersson, J.: A review of the parameter estimation problem of fitting positive exponential sums to empirical data. Appl. Math. Comput. **126**(1), 31–61 (2002)
15. Kienzler, R., Herrmann, G.: Mechanics in Material Space: with Applications to Defect and Fracture Mechanics. Springer, Berlin (2012)
16. Kim, K.S., Aravas, N.: Elastoplastic analysis of the peel test. Int. J. Solids Struct. **24**(4), 417–435 (1988)

17. Maugin, G.A.: Material Inhomogeneities in Elasticity. Chapman Hall, London (1993)
18. Menga, N., Afferrante, L., Pugno, N., Carbone, G.: The multiple V-shaped double peeling of elastic thin films from elastic soft substrates. J. Mech. Phys. Solids **113**, 56–64 (2018)
19. Nase, M., Langer, B., Baumann, H.J., Grellmann, W., Geißler, G., Kaliske, M.: Evaluation and simulation of the peel behavior of polyethylene/polybutene-1 peel systems. J. Appl. Polym. Sci. **111**(1), 363–370 (2009)
20. Nase, M., Langer, B., Grellmann, W.: Fracture mechanics on polyethylene/polybutene-1 peel films. Polym. Testing **27**(8), 1017–1025 (2008)
21. Nase, M., Rennert, M., Henning, S., Zankel, A., Naumenko, K., Grellmann, W.: Fracture mechanics characterisation of peelfilms. In: Deformation and Fracture Behaviour of Polymer Materials, pp. 271–281. Springer (2017)
22. Nase, M., Rennert, M., Naumenko, K., Eremeyev, V.A.: Identifying traction-separation behavior of self-adhesive polymeric films from in situ digital images under t-peeling. J. Mech. Phys. Solids **91**, 40–55 (2016)
23. Nase, M., Zankel, A., Langer, B., Baumann, H.J., Grellmann, W., Poelt, P.: Investigation of the peel behavior of polyethylene/polybutene-1 peel films using in situ peel tests with environmental scanning electron microscopy. Polymer **49**(25), 5458–5466 (2008)
24. Naumenko, K., Eremeyev, V.A.: A layer-wise theory of shallow shells with thin soft core for laminated glass and photovoltaic applications. Compos. Struct. **178**, 434–446 (2017)
25. Needleman, A.: Some issues in cohesive surface modeling. Procedia IUTAM **10**, 221–246 (2014)
26. Park, K., Paulino, G.H.: Cohesive zone models: a critical review of traction-separation relationships across fracture surfaces. Appl. Mech. Rev. **64**(6), 060802 (2011)
27. Pettersson, S., Engqvist, J., Hall, S., Toft, N., Hallberg, H.: Peel testing of a packaging material laminate studied by in-situ x-ray tomography and cohesive zone modeling. Int. J. Adhes. Adhes. **95**, 102428 (2019)
28. Potts, D., Tasche, M.: Nonlinear approximation by sums of nonincreasing exponentials. Appl. Anal. **90**(3–4), 609–626 (2011)
29. Rivlin, R.S.: The effective work of adhesion. In: G.I. Barenblatt, D.D. Joseph (eds.) Collected Papers of R.S. Rivlin, vol. 2, pp. 2611–2614 (1997)
30. Ruybalid, A., Hoefnagels, J., van der Sluis, O., van Maris, M., Geers, M.: Mixed-mode cohesive zone parameters from integrated digital image correlation on micrographs only. Int. J. Solids Struct. **156**, 179–193 (2019)
31. Wei, Y., Hutchinson, J.: Interface strength, work of adhesion and plasticity in the peel test. Int. J. Fract. **1**(93), 315–333 (1998)
32. Weps, M., Naumenko, K., Altenbach, H.: Unsymmetric three-layer laminate with soft core for photovoltaic modules. Compos. Struct. **105**, 332–339 (2013)
33. Williams, J., Hadavinia, H.: Analytical solutions for cohesive zone models. J. Mech. Phys. Solids **50**(4), 809–825 (2002)
34. Yim, M.J., Paik, K.W.: Recent advances on anisotropic conductive adhesives (ACAs) for flat panel displays and semiconductor packaging applications. Int. J. Adhes. Adhes. **26**(5), 304–313 (2006)